Journal of King Saud University – Science 35 (2023) 102620

HOSTED BY

Contents lists available at ScienceDirect

Journal of King Saud University – Science

journal homepage: www.sciencedirect.com

Review

# Investigating the properties and biological activity of a new Cu(II) complex with a 2-Dimethyaminopyridinium cation $(C_7H_{12}N_2)_2[CuCl_4]$

Abdullah A. Alotaibi

*Department of Chemistry, College of Science and Humanities, Shaqra University, 11911 Ad-Dawadmi, Saudi Arabia*

ARTICLE INFO

*Article history:*
Received 23 September 2022
Revised 5 February 2023
Accepted 20 February 2023
Available online 25 February 2023

*Keywords:*
Cu (II) complex
Single crystal
X-ray diffraction
FT-IR spectroscopy
Hirshfeld surface
Biological activity

ABSTRACT

A new single crystal of $(C_7H_{12}N_2)_2[CuCl_4]$ was developed at room temperature using the gradual evaporation technique, resulting in an interesting structural arrangement. The crystal is composed of alternating organic and inorganic layers that are held together by the cohesive force of H-bonds formed between the organic and inorganic groups, as well as interactions controlled by Van der Waals forces. The distribution of intermolecular interactions was explored using Hirshfeld surface analysis, revealing that H...H contacts make up a substantial portion of the Hirshfeld surface. To uncover the vibrational features of this structure, infrared spectroscopy was employed, and the vibrational bands were assigned by comparing the frequencies to those of similar compounds. With the increasing issue of multi-drug-resistant bacteria, the potential for a synergistic effect between antibiotics and metal ion complexes is becoming more critical. This was tested by combining antibiotics with $(C_7H_{12}N_2)_2[CuCl_4]$ and investigating their antibacterial activity using disk diffusion techniques, which showed a synergistic increase in activity against opportunistic nosocomial pathogen bacterial strains.



**Contents**



Peer review under responsibility of King Saud University.

Production and hosting by Elsevier

*E-mail address:* aaalotaibi@su.edu.sa

https://doi.org/10.1016/j.jksus.2023.102620
1018-3647/

## 1. Introduction

Recently, there has been an incredible advancement in the study of medicinal chemistry, with a particular focus on the research of metal compounds, which have been used to control many different kinds of diseases (Krasnovskaya et al., 2020). For therapeutic reasons, Cu (II) is one of the most significant metal ions in biological systems. It is indeed playing a key role in physiological processes involving ceruloplasmin, albumin, and other proteins (Oliveri, 2020; Duncan and White, 2012). Copper may serve as an antioxidant too, by neutralizing free radicals and perhaps preventing some of the harm they cause, as well as contributing to the development of Alzheimer's disease (Robert et al., 2015; Krajčiová et al., 2014). Furthermore, Cu-containing metallic materials demonstrated exceptional cardiovascular and antimicrobial activity (Schmidt et al., 2017; Wang et al., 2021). Thus, we designed the pyridine moiety, an important heterocyclic pharmacophore with tremendous applications (Mali and Chaudhari, 2018; Zakharychev et al., 2020), especially in the field of agrochemical products (Guan et al., 2016). Current interest in pyridine and its derivatives stems from its prospective use as an antimicrobial, antidiabetic, anti-inflammatory, anticonvulsant, and antitumor agent (Kamat et al., 2020; Prachayasittikul et al., 2017).

Given the importance of Cu(II) and the pharmacological significance of pyridine, copper (II) compounds are an important class in chemistry not only for their intrinsically interesting properties but also for their widespread application (Althobaiti et al., 2022; Mohammad Abu-Taweel et al., 2022). These latter are well recognized because of their immense biological significance as anticancer, anti-inflammatory (Psomas, 2020), anti-tuberculosis (Buczkowska et al., 2011), antioxidant agents (Ragab et al., 2022) and exceptional activity with toxicity profiles (Smolková et al., 2017; Sunitha et al., 2020; Khan et al., 2021; Hashem et al., 2022; Himasekar et al., 2019). Additionally, the coordination of antibiotics with certain transition metals is known to increase their antimicrobial activity.

Our research focuses on the characterization of the crystal structure and vibrational properties of a novel hybrid material, bis-(2-dimethylaminopyrimidinium) tetrachloridecuprate (II). Then, we look into the antibacterial activity of some pathogenic bacteria strains.

## 2. Experimental and methodology

### 2.1. $(C_7H_{12}N_2)_2[CuCl_4]$ preparation

$(C_7H_{12}N_2)_2[CuCl_4]$ or bis-(2-dimethylaminopyrimidinium) tetrachloridecuprate (II) (Mw = 453.71 g.mol$^{-1}$) was synthesized by the slow evaporation technique. An aqueous solution of $CuCl_2 \cdot 2H_2O$ (1 mmol) and 2-dimethylaminopyridine (2 mmol in 5 mL of pure ethanol) were mixed in a round-bottom flask. Then, 10 mL of concentrated hydrochloric acid was added to the solution, which was allowed to stir mechanically for about two hours at 50 °C. After a few days of progressively evaporating, prismatic crystals appropriate for X-ray research were formed. Recrystallization of the crystals from the water was required to increase their quality.

### 2.2. Instrumentation

#### 2.2.1. SEM/EDX examinations and powder X-ray diffraction

In the remaining portion of our investigation, we employed a wide range of methods to investigate $(C_7H_{11}N_2)_2CuCl_4$. The SEM/EDX was used to examine the crystal structure and elemental composition of the title chemical, which were carried out at 15 KV utilizing a JEOL-JSM 6610LV EDX detection system instrumentation piece. In addition, the XRD powder pattern was generated using a Siemens D5000 XRD system equipped with a Cu anticathode (1.54056).

#### 2.2.2. Single crystal X-ray diffraction analysis

On a Calibur Ruby Gemini diffractometer equipped with Mo-Kα radiation (0.71073) at room temperature, diffraction data from a single crystal was recorded at ambient temperature. The CrysAlis PRO software was used to analyze the data (Betteridge et al., 2003), and the setting angles of 3555 reflections were used in the process of adjusting the lattice parameters, with θ between 2.5 and 19.2. Analytical numeric absorption adjustments were used to create empirical absorption corrections. Analyses of the structure were done with monoclinic symmetry and the space group C2/c. The full-matrix least squares approach (SHELXL-97 software) was used to refine the data and it converged to an appropriate final agreement factor (Sheldrick, 2008). Anisotropic temperature parameters were used to refine all non-hydrogen atoms. Table 1 shows the refined and crystallographic data.

**Table 1**
The crystallographic results for $(C_7H_{12}N_2)_2[CuCl_4]$.

| **Crystal Data** | |
|---|---|
| Chemical Formula | $(C_7H_{12}N_2)_2$ $[CuCl_4]$ |
| $M_r$ (g.mol$^{-1}$) | 453.71 |
| Crystal System, Space group | Monoclinic, C2/*c* |
| Temperature (K) | 298 |
| a (Å) | 34.336 (4) |
| b (Å) | 8.5501 (6) |
| c (Å) | 16.346 (2) |
| β (°) | 124.60 (2) |
| V (Å$^3$) | 3949.9 (11) |
| Z | 8 |
| Radiation type | Mo*K*α radiation |
| μ (mm$^{-1}$) | 1.65 |
| Crystal size (mm) | 0.12 × 0.1 × 0.05 |
| Form, Color | Prism, Colorless |
| **Data Collection** | |
| Diffractometer | Xcalibur, Ruby, Gemini |
| Absorption correction | Analytical |
| $\theta_{min}$, $\theta_{max}$ (°) | 2.5–25.2 |
| No. of measured, and observed [I > 2σ(1)] reflections | 6799, 1661 |
| $R_{int}$ | 0.143 |
| $(\sin\theta/\lambda)_{max}$ (Å$^{-1}$) | 0.599 |
| **Refinement** | |
| R[F$^2$ > 2σ(F$^2$)], wR(F$^2$) S | 0.115, 0.183, 1.12 |
| No. of reflections | 3555 |
| No. of parameters | 265 |
| No. of restraints | 246 |
| $\Delta\rho_{min}$, $\Delta\rho_{max}$ (e.Å$^3$) | −0.39, 0.40 |
| **CCDC No.** | 2,203,998 |

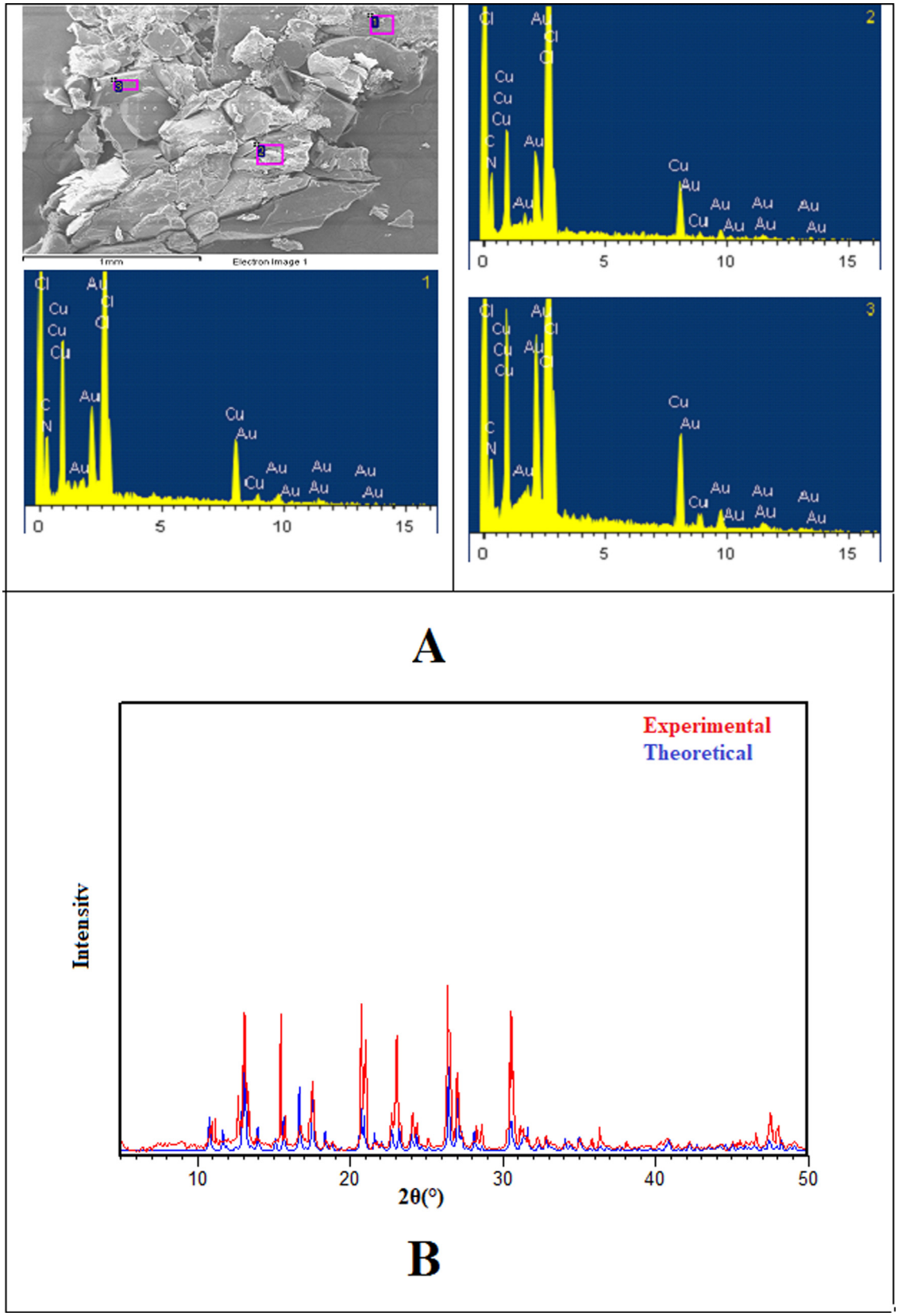


**Fig. 1.** SEM image observation and related EDX analysis from three separate zones (A) and experimental and theoretical X-ray diffractograms of $(C_7H_{12}N_2)_2[CuCl_4]$ (B).

*2.2.3. Hirshfeld surface analysis*

Many studies have shown the usefulness of visualizing a surface using the Hirshfeld method. Surfaces were mapped with various attributes, and the 2D fingerprint maps were generated via CrystalExplorer 17.5 software, (Spackman et al., 2021) in order to examine intermolecular interactions in this compound.

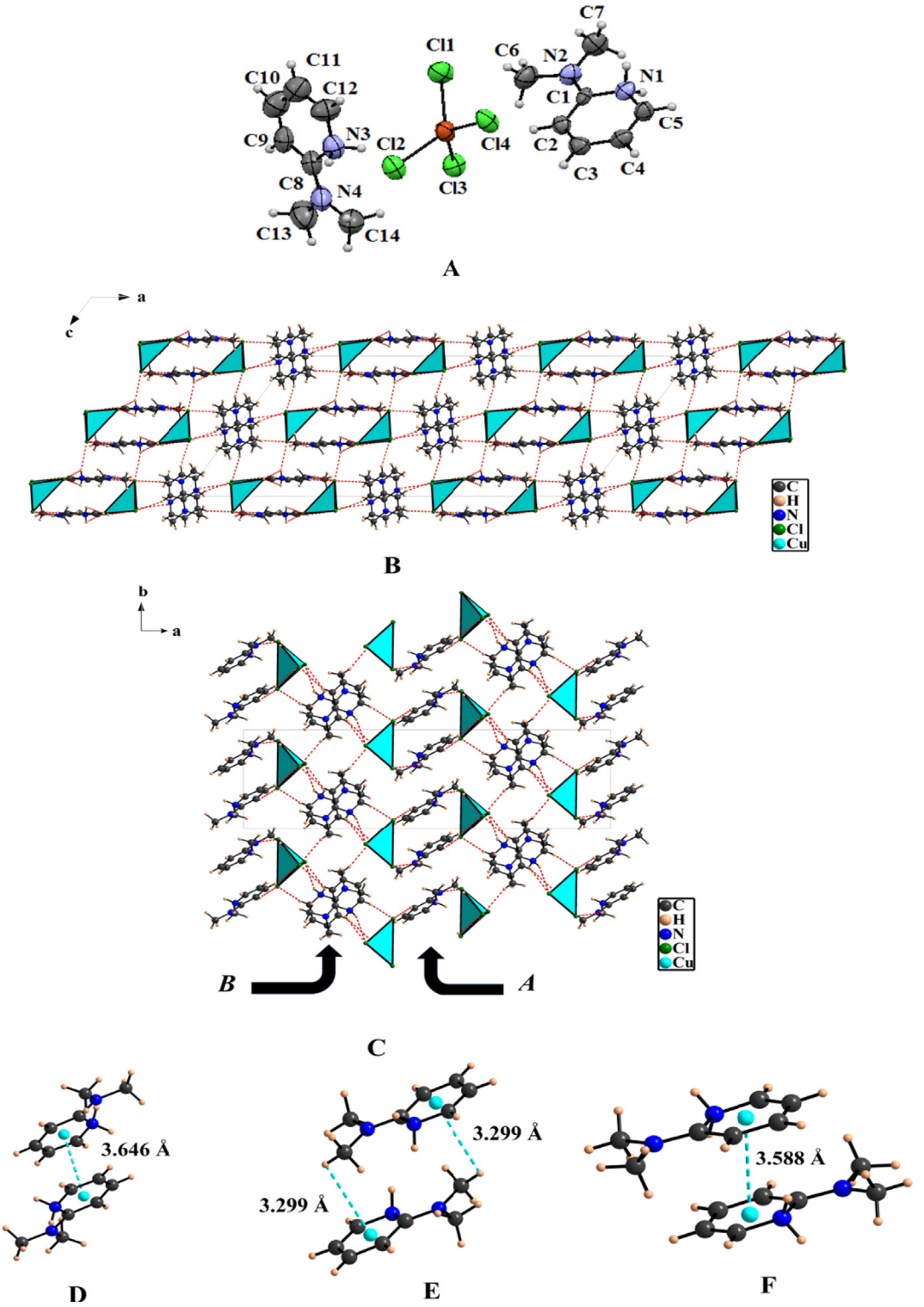


**Fig. 2.** $(C_7H_{12}N_2)_2[CuCl_4]$ structure projection along the b-axis (A), atomic arrangement parallel to the [0 0 1] direction (B), interaction between two cations type A (C), C–H. . . π interaction (D) π. . .π, and interaction between two cations type B (E).

*2.2.4. Antibacterial activity*

The disc diffusion technique was utilized to assess the antibacterial activity of $(C_7H_{12}N_2)_2[CuCl_4]$ against Klebsiella pneumonia, Serratiamarcescens, and Staphylococcus aureus, as well as its synergistic impact when combined with antibiotics (NOR-10; Novobiocin (NV-5); Erythromycin (E-15) and Nalidixic acid (NA30)). The disc diffusion procedure was performed in accordance with the guidelines provided by the NCCLS (National Committee for Clinical Lab Standards). In fact, the whole nutritional agar (Scharlau Microbiology) was swabbed with each bacterial strain's inoculum suspension, where the four dilutions of substance were poured into the three bacterial strain plates using sterile 4 mm filter paper discs. However, allowing for extra pre-diffusion, after 15 min at room temperature, the plates were incubated at 37 °C for 24 h. A solution of $(C_7H_{12}N_2)_2[CuCl_4]$ was dipped into the discs of Norfloxacin (NOR-10); Novobiocin (NV-5); Erythromycin (E-15) and

**Table 2**
H-bonds for $(C_7H_{12}N_2)_2[CuCl_4]$.

| D—H...*A* | D—H (Å) | H...*A*(Å) | D...H (Å) | D—H...*A*(°) |
|---|---|---|---|---|
| **N1—H1...Cl4** | 0.89 | 2.76 | 3.2259 | 114 |
| **N3—H3A...Cl2** | 0.89 | 2.75 | 3.2419 | 116 |
| **C2—H2...Cl3** | 0.93 | 2.80 | 3.6819 | 159 |
| **C5—H5...Cl1** | 0.93 | 2.68 | 3.5968 | 168 |
| **C7—H7B...Cl3** | 0.96 | 2.82 | 3.7179 | 156 |
| **C9—H9...Cl1** | 0.93 | 2.63 | 3.6714 | 151 |
| **C10—*H*10...Cl3** | 0.93 | 2.74 | 3.6544 | 167 |
| **C11—*H*11...Cl1** | 0.93 | 2.81 | 3.6986 | 161 |

**Table 3**
Experimental geometrical parameters of bis-(2-dimethylaminopyrimidinium) tetrachloridecuprate (II).

| Distances (Å) | | Angles (°) | |
|---|---|---|---|
| **$[CuCl_4]^{2-}$** | | | |
| | | Cl3-Cu1-Cl1 | 100.19 (12) |
| Cu1-Cl1 | 2.247 (3) | Cl3-Cu1-Cl4 | 133.09 (12) |
| Cu1-Cl2 | 2.275 (3) | Cl1-Cu1-Cl4 | 100.33 (12) |
| Cu1-Cl3 | 2.242 (3) | Cl3-Cu1-Cl2 | 99.79 (12) |
| Cu1-Cl4 | 2.259 (3) | Cl1-Cu1-Cl2 | 128.73 (12) |
| | | Cl4-Cu1-Cl2 | 99.35 (11) |
| **$(C_7H_{12}N_2)^+$** | | | |
| C1—N1 | 1.379 (9) | C2—C3—C4 | 119.5 (9) |
| C1—N2 | 1.306 (10) | C5—C4—C3 | 120.2 (10) |
| C5—N1 | 1.366 (10) | C4—C5—N1 | 119.0 (10) |
| C6—N2 | 1.462 (10) | C5—N1—C1 | 123.9 (8) |
| C7—N2 | 1.442 (11) | C1—N2—C7 | 123.2 (8) |
| C8—N4 | 1.320 (16) | C1—N2—C6 | 121.1 (8) |
| C8—N3 | 1.388 (14) | C7—N2—C6 | 115.4 (8) |
| C12—N3 | 1.385 (18) | N4—C8—C9 | 122.8 (15) |
| C13—N4 | 1.438 (16) | N4—C8—N3 | 119.7 (14) |
| C14—N4 | 1.440 (17) | C9—C8—N3 | 117.2 (15) |
| C15—N6 | 1.319 (19) | C10—C9—C8 | 121.0 (16) |
| C15—N5 | 1.394 (16) | C9—C10—C11 | 120.1 (17) |
| C19—N5 | 1.374 (19) | C12—C11—C10 | 120.9 (18) |
| C20—N6 | 1.448 (18) | C11—C12—N3 | 118.4 (17) |
| C21—N6 | 1.441 (19) | C12—N3—C8 | 122.3 (14) |
| C1—C2 | 1.391 (11) | C8—N4—C13 | 122.3 (15) |
| C2—C3 | 1.354 (11) | C8—N4—C14 | 121.0 (14) |
| C3—C4 | 1.412 (12) | C13—N4—C14 | 116.7 (16) |
| C4—C5 | 1.325 (11) | N6—C15—C16 | 125 (2) |
| C8—C9 | 1.388 (15) | N6—C15—N5 | 118.3 (19) |
| C9—C10 | 1.337 (19) | C16—C15—N5 | 115.6 (19) |
| C10—C11 | 1.413 (19) | C17—C16—C15 | 122 (2) |
| C11—C12 | 1.330 (18) | C16—C17—C18 | 120 (2) |
| C15—C16 | 1.391 (17) | C19—C18—C17 | 121 (2) |
| C16—C17 | 1.34 (2) | C18—C19—N5 | 118 (2) |
| C17—C18 | 1.41 (2) | C19—N5—C15 | 123.5 (18) |
| C18—C19 | 1.33 (2) | C15—N6—C21 | 124 (2) |
| | | C15—N6—C20 | 121 (2) |
| | | C21—N6—C20 | 115 (2) |

Nalidixic acid (NA30) to investigate the synergistic impact of our produced chemical and the employed antibiotics. The widths of the inhibitory zones were then measured, either alone or in combination with antibiotics. Finally, it is worth mentioning that Norfloxacin (NOR-10); Novobiocin (NV-5); Erythromycin (E-15) and Nalidixic acid (NA30) were utilized as experimental positive controls in a microbiological susceptibility control test.

## 3. Results and discussion

### 3.1. Powder XRD and SEM/EDX observations

SEM image examination reveals that the hybrid's surfaces seem to be flat. Areas of strong contrast were used for EDX analysis during SEM. To verify the existence of heavy element compositions in the crystal. As may be seen by the presence of the typical signals from the elements carbon, copper, chloride, and nitrogen (Fig. 1**A**). In addition, there were no differences discovered between the simulated and experimental XRPD patterns of $(C_7H_{12}N_2)_2[CuCl_4]$ when comparing both sets (Fig. 1**B**). This provides further evidence that the product that was synthesized is pure and confirms the crystal data that was used in the process of synthesizing it.

### 3.2. Structure of the crystal

Fig. 2**A** shows the asymmetric unit of the structure generated with 50% probability thermal ellipsoids for non-hydrogen atoms, which contains two non-equivalent cations: bis-(2-dimethylamino pyrimidinium) tetrachloridecuprate (II) (cation A made up by: C8-C12/N3, and cation B made by: C1-C5/N1) and one tetrahedron anions $[CuCl_4]^{2-}$. As can be observed, the N atoms of the pyridine ring are protonated, whilst the amine groups remain unprotonated. Therefore, the charge of each organic cation is increased by + 1. As a result, the structure matches each tetrachlorocuprate anion with two 2-dimethylaminopyridinium cations in order to preserve the charge balance.

$(C_7H_{12}N_2)_2[CuCl_4]$ packing along the b-axis reveals that the title compound's structure is made up of mixed cation–anion layers that run parallel to the (1 1 0) plane and are held together by C11-*H*11...Cl1 H-bonds and Van der Waals interactions. The H-bonds, on the other hand; C5-H5...Cl1, C9-H9... Cl1, N3-H3A, Cl2, C7-H7B, Cl3, C2-H2... Cl3, C10-*H*10... Cl3 and Cl4 connect two neighboring layers to form a three-dimensional network (Table 2, Fig. 2**B**).

A mixed layer is formed by paralleling organic (cations type A) and inorganic columns to the [0 1 0] axis (Fig. 2**C**). Cations A generate organic columns with centroids spaced at 3.646 (Fig. 2**D**) and C—H... π interactions (3.299 Å) (Fig. 2**E**), whereas cations B interact via offset face-to-face π...π interactions with centroids spaced at 3.588 Å (Fig. 2**F**).

The geometric characteristics of organic cations $(C_7H_{12}N_2)^{2+}$ are listed in Table 3. These findings are consistent with those seen in similar compounds (Kumar et al., 2020; Sundaraganesan et al., 2008; Szafran et al., 2005). The sum of the angles that surround the nitrogen atoms N(4) and N(2) in the cations A and B, respectively, is close to being equal to 360°. The C—N bond distance of the $NH_2$ group is 1.320 (16) Å for cation A and 1.306 (10) Å for cation B. This distance is consistent with an imino resonance form, which is often seen for a C—N single bond containing $sp^2$ hybridized C and N atoms. The delocalization of the ring density with the p-orbital electrons of the amino group is most likely the cause of the decrease in the distance between the C—N amino bond and the amino group. Because of this, the basicity of the nitrogen atoms at positions N(2) and N (4) decreases, which makes protonation of the nitrogen atoms at positions N(1) and N(3) on the pyridine ring more likely. A pyridinium cation will almost always have a larger C—N—C angle when compared to the parent pyridine molecule. Both the C1—N1—C5 angle of 120.83 (10) ° and the C8—N3—C12 angle of 122.3 (14) °

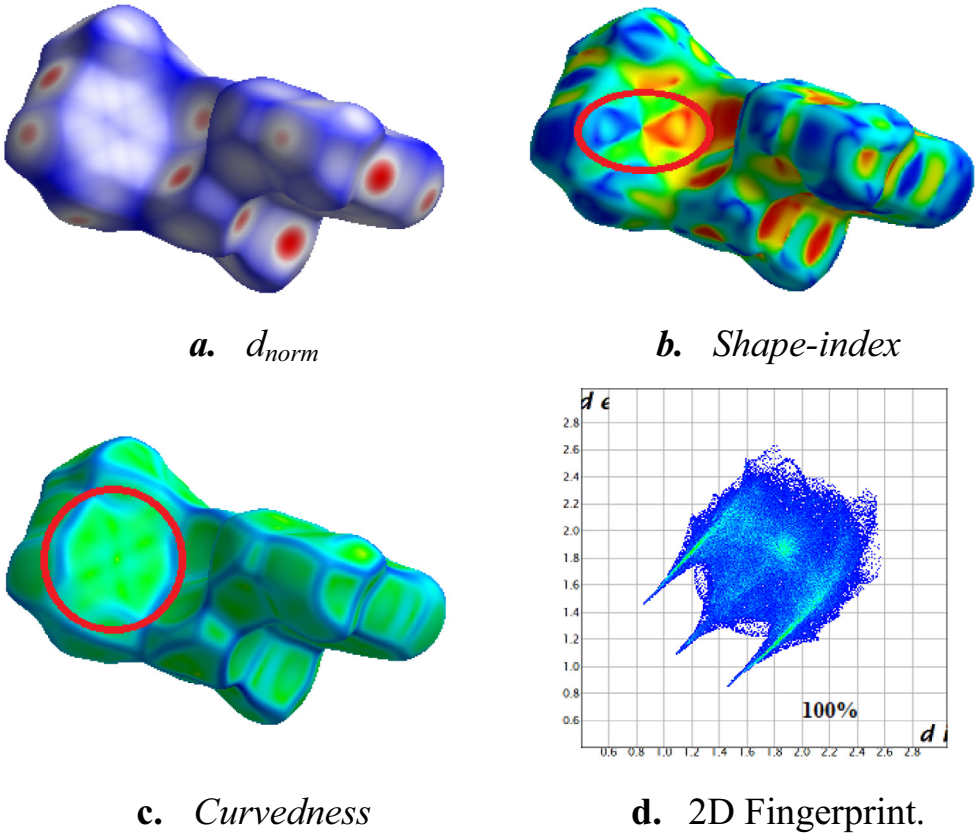


**Fig. 3.** Hirshfeld surface mapped with dnorm (a), shape index (b), curvedness (c), 2D fingerprint plots (d).

**Table 4**
$E_{XY}$'s reports for bis-(2-dimethylaminopyrimidinium) tetrachloridecuprate (II).

| Atoms | Cu | Cl | N | C | H |
|---|---|---|---|---|---|
| **% Surface** | 0.55 | 18.75 | 2.55 | 6.45 | 71.7 |
| **Cu** | | | | | 1.39 |
| **Cl** | | | 0.94 | 0.16 | 1.35 |
| **N** | | 0.94 | 6.15 | 3.34 | 0.63 |
| **C** | | 0.16 | 3.34 | 3.60 | 0.91 |
| **H** | 1.39 | 1.35 | 0.63 | 0.91 | 0.93 |

are typical for the protonated forms of pyridine that have been described in the literature (Vembu et al., 2003; Majerz et al., 1995).

The Cu—Cl distances of the tetrahedrally coordinated $[CuCl_4]^{2-}$-anion range from 2.242 (3) to 2.275 (3) Å and the angle Cl—Cu—Cl ranges between 99.35 (11) ° and 133.09 (12) °. These bonding lengths and angles are consistent with those observed in other compounds (Table 3) (Nasr et al., 2016; Halvorson et al., 1990).

The values for dissociation constants (DI) were as follows: DI (Cl—Cu) = 0.0049, DI(Cl—Cl) = 0.078, and DI(Cl—Cu—Cl) = 0.124. In comparison to Cl—Cl distances, the angles Cl—Cu—Cl in these measurements are significantly distorted. The anions $[CuCl_4]^{2-}$ are thought to be made up of chlorine atoms in a regular configuration, with the copper atom slightly dislocated from the tetrahedron's center of gravity. Additionally, the Yang parameter $\tau_4$ may be utilized, with a value of zero suggesting a perfect square planar geometry and a value of one indicating a perfect tetrahedral geometry (Yang et al., 2007). The estimated value of 0.69 indicates that the tetrachlorocuprate anions have almost a tetrahedral structure.

### 3.3. HS surface study

The Hirshfeld surface (HS) is drawn over the $d_{norm}$ surface to find the interactions between molecules in the complex's solid phase structure (Fig. 3**a**). The blue sections indicate distances greater than the total of the van der Waals radii of the associated atoms, while the red parts indicate lesser distances. The circular red spots are actually caused by the N—H. . .Cl and C–H. . .Cl connections, while the white spots are caused by other contacts. The HS shape-index is used to visualize the π. . .π stacking by detecting the presence of adjacent red and blue triangles (Fig. 3**b**). The title structure, $(C_7H_{12}N_2)_2[CuCl_4]$, clearly demonstrates the presence of π. . .π stacking interactions, where a flat region surrounding the pyridine rings on the Hirshfeld surface, plotted against curvedness (Fig. 3**c**). Moreover, the 2D fingerprint graphs can be used to separate the interactions between molecules in a structure, which makes it possible to observe how much each one contributes. The overall two-dimensional fingerprint pattern is shown in Fig. 3**d**.

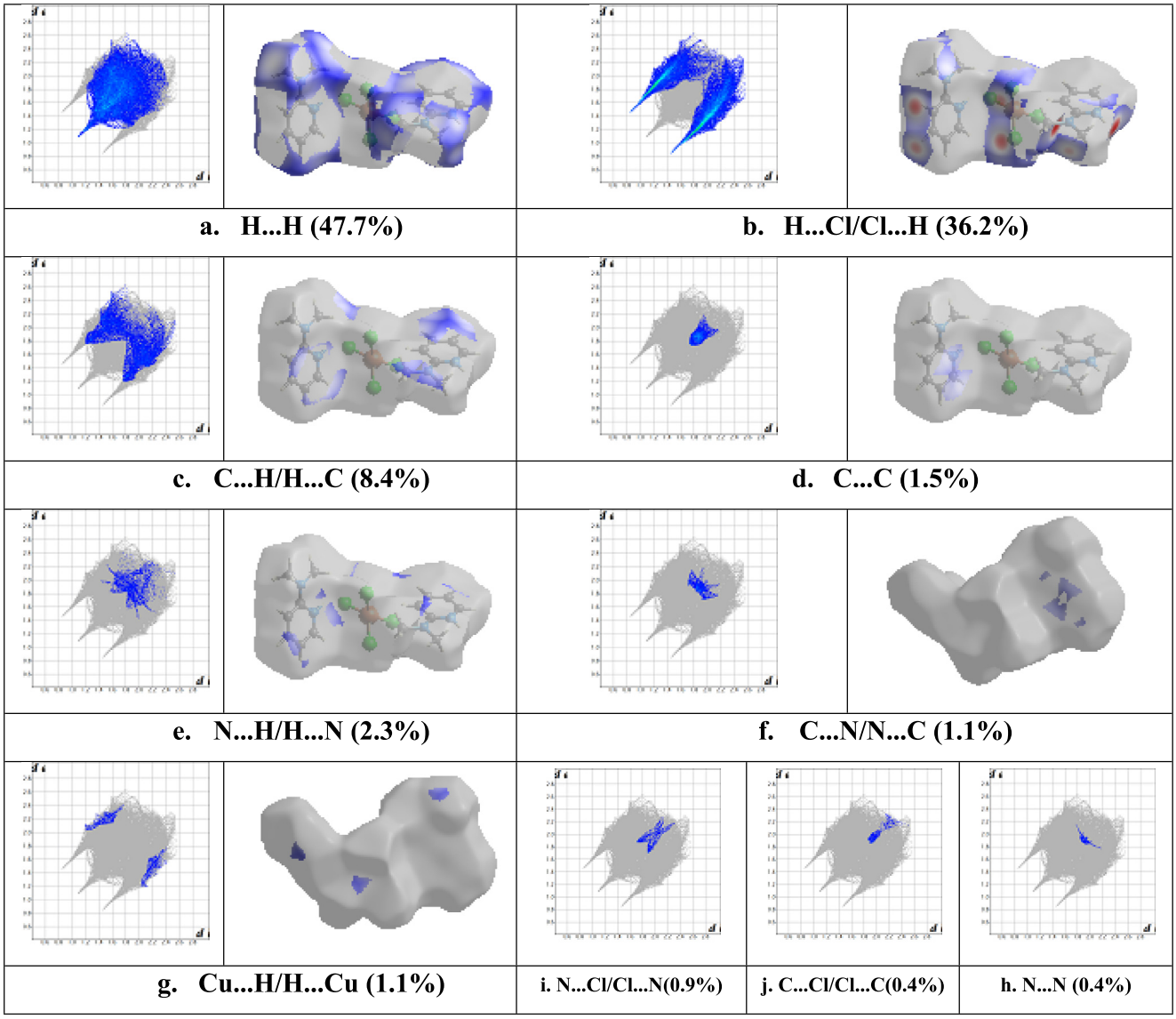


**Fig. 4.** The 2D fngerprint map for $(C_7H_{12}N_2)_2[CuCl_4]$ illustrating the contribution all contacts.

Fig. 3**d** depicts the 2D fingerprint of all contacts contributing to the Hirshfeld surface. The enrichment ratio computation for a pair of elements (X, Y) $E_{XY}$ is presented in Table 4. According to the plot shown in Fig. 4**a** H. . .H are the most frequently detected interactions, with a relative contribution of 47.7%.and with an enrichment ratio slightly under-represented by $E_{H\ldots H}$ = 0.92. The H. . .Cl/Cl. . .H interactions account for 36.2% of the total HS area (Fig. 4**b**).Due to the abundance of chloride and hydrogen on the molecular surface ($S_{Cl}$ = 18.75% and $S_H$ = 71.7%), these are significantly favored with an enrichment ratio of $E_{H\ldots Cl}$ = 1.35. The C. . .H/H. . .C interactions account for 8.4% of the overall area (Fig. 4**c**), and are preferred contact in the crystal packing ($E_{C\ldots H}$ = 0.91). The hydrophobic C. . .C contacts account for 1.5% of the overall surface area (Fig. 4**d**) and are considered as more pronounced since the associated enrichment ratio is $E_{C\ldots C}$ = 3.60 as a result of π. . .π stacking between the aromatic pyridine rings. In contrast, the N. . .H interactions make about 2.3% of the Hirshfeld surface (Fig. 4**e**), followed by C. . .N/N. . .C and Cu. . .H/H. . .Cu that both count for 1.1% of the whole Hirshfeld surface area (Fig. 4**f** and Fig. 4**g**). However, the N. . .Cl/Cl..N (Fig. 4**h**), C..Cl/Cl. . .C (Fig. 4**i**), and N. . .N (Fig. 4**f**) contacts, each contribute around 0.9%, 0.4%, and 0.4% of the total surface, respectively, and are particularly poor. It is important to note that the remaining contributions do not accurately reflect their contribution to the structure's stabilization.

We conclude from this analysis that H. . .H and Cl. . .H contacts, followed by C. . .H, account for most of the total surface, reflecting the driving force in this crystal packing.These findings support the notion that the presence of π. . .π stacking, C—H. . .interactions, and H-bonds plays an important role in the stability of crystalline structures (Munawar et al., 2023; Chalkha et al. 2023). Therefore, the absence of these interactions in solution may be a contributing factor to instability and subsequent dissociation.

### 3.4. IR-Spectroscopy of $(C_7H_{12}N_2)_2[CuCl_4]$

Fig. 5 depicts the IR spectra of $(C_7H_{12}N_2)_2[CuCl_4]$, which is in excellent agreement with the structural X-ray study findings. The different vibrational modes of this compound are compared with other compounds having the same organic cation (Karaa et al., 2012; Thanigaimani et al., 2015). The two bands located at 3068

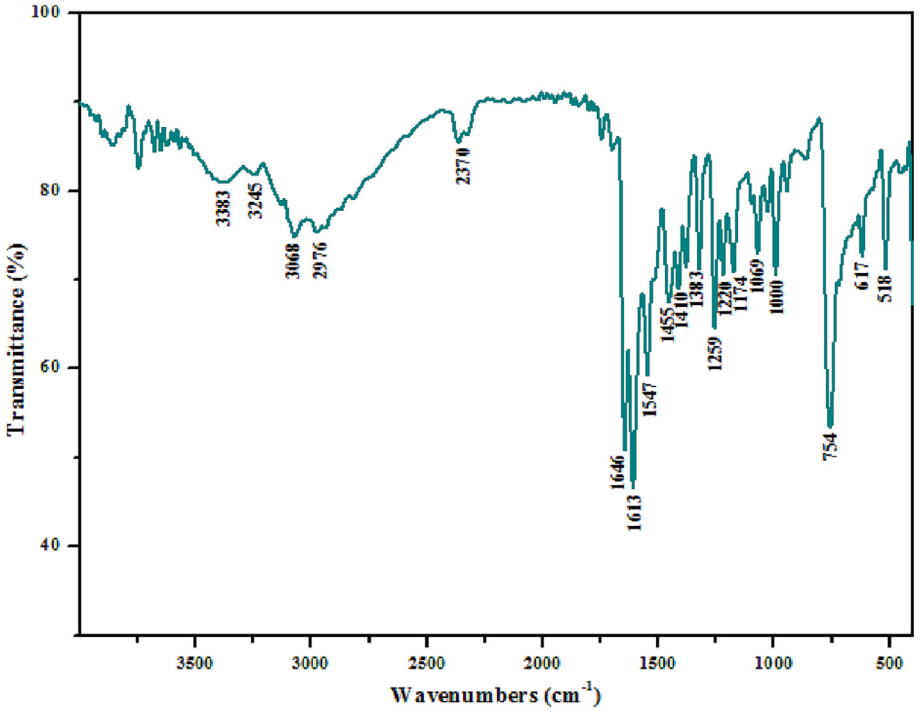


**Fig. 5.** The infrared spectrum of $(C_7H_{12}N_2)_2[CuCl_4]$ at room temperature.

and at 2976 $cm^{-1}$ correspond to the vibrations of asymmetric lengthening of the C—H bond of the methyl groups-CH3 and of the C—H bond of the aromatic ring. The pyridinium N—H group's elongation vibrations can be at 3383 $cm^{-1}$and at 3245 $cm^{-1}$, on the other hand, the two peaks located at 1646 and at 1613 $cm^{-1}$ are attributed to the deformation vibrations δ(N—H). The stretching vibration of the C=C bond in the infrared spectrum of the title compound is characterized by a peak observed at 1547 $cm^{-1}$.

The –CH3 groups' deformation vibrations are positioned by three successive bands, the first at 1455 cm-1, the second at 1410 cm-1, and the last at 1383 $cm^{-1}$. Frequencies between 1259 and 1000 $cm^{-1}$ are assigned to the vibrations of ν (C—N) and ν (C—C). The remains of the bands (between 1000 and 400 $cm^{-1}$) are attributed to the out-of-plane bending modes for C—H, C—C and C—N bonds.

### 3.5. Antibacterial activity

Using the disc diffusion method, different concentrations of bis-(2-dimethylaminopyrimidinium) tetrachloridecuprate (II); 100 μg. $mL^{-1}$; 50 μg.$mL^{-1}$; 25 μg.$mL^{-1}$ and 12.5 μg.$mL^{-1}$ were tested against three opportunistic nosocomial pathogen bacterial strains: *Klebsiella pneumonia* and *Serratiamarcescens*, which are both gram-negative; and *Staphylococcus aureus*, which is a Gram-positive bacterial strain (Sarangi et al., 2020; Azam et al., 2021; Azam et al., 2022; Al-Resayes et al., 2017). The zone (mm) of inhibition, the compound showed high antibacterial activity against *Serratiamarcescens* even in small concentration 12.5 μg.$mL^{-1}$, whereas the antibiotics control Norfloxacin (NOR-10) and Nalidixic acid (NA30) did not inhibit cell viability but Novobiocin (NV-5); Erythromycin (E-15) agent, was observed either by using high concentrations of 50 g.$mL^{-1}$ and 100 μg.$mL^{-1}$ from the compound $(C_7H_{12}N_2)_2[CuCl_4]$ or by the four used antibiotics (Fig. 6). The combination of the compound $(C_7H_{12}N_2)_2[CuCl_4]$ with the four antibiotics was tested against two Gram-negative bacterial strains (*Klebsiella pneumonia* and *Serratiamarcescens*) and Gram- positive bacteria (*Staphylococcus aureus*) using the disc diffusion method. The zone of inhibition (mm) of different antibiotic discs with $(C_7H_{12}N_2)_2[CuCl_4]$ against test three strains was measured and revealed that the free compound or the reference used four antibiotics had the highest antimicrobial activity. A Copper (II) complex with 12.5 μg. $mL^{-1}$ produced a maximum fold increase of 60% antibacterial activity against *Serratiamarcescens*. In the case of *Klebsiella pneumonia* and *Staphylococcus aureus,* the synthesized compound 100 μg.$mL^{-1}$ together with the antibiotics shows as 10% fold increase against both strains. In the current investigation, the antibiotics' synergistic efficacy against the three different pathogens was significantly increased in the presence of $(C_7H_{12}N_2)_2[CuCl_4]$.

The increasing antimicrobial activity of Cu (II) compounds can be explained by the cell permeability. Because the lipid membrane surrounding the cell preferred only fat-soluble substances to pass, fat solubility is an important factor in antimicrobial control activity. Cu (II) increases the lipophilic character of the central metal atom, allowing it to penetrate the cellular fat layers membrane and inhibit bacterial growth (Anjaneyulu and Prabhakara Rao, 1986; Chandraleka et al., 2014).

## 4. Conclusion

For this study, we synthesized $(C_7H_{12}N_2)_2[CuCl_4]$ and analyzed its physical–chemical properties. At room temperature, this chemical crystallizes in the monoclinic, system (C2/*c* space group). Our compound's crystal packing is determined by N—H...Cl, C—H...Cl H-bonds, π...π and C—H...π interactions. The Hirshfeld surface (HS) analysis in the form of deconstructed fingerprint plots allowed for the decoding of these types of intermolecular interactions. Organic and inorganic groups are confirmed by FT-infrared investigations. Antibiotics were added to the compound $(C_7H_{12}N_2)_2[CuCl_4]$ and antibacterial activity was determined using disk diffusion techniques, demonstrating a synergistic enhancement in action against opportunistic nosocomial pathogens.

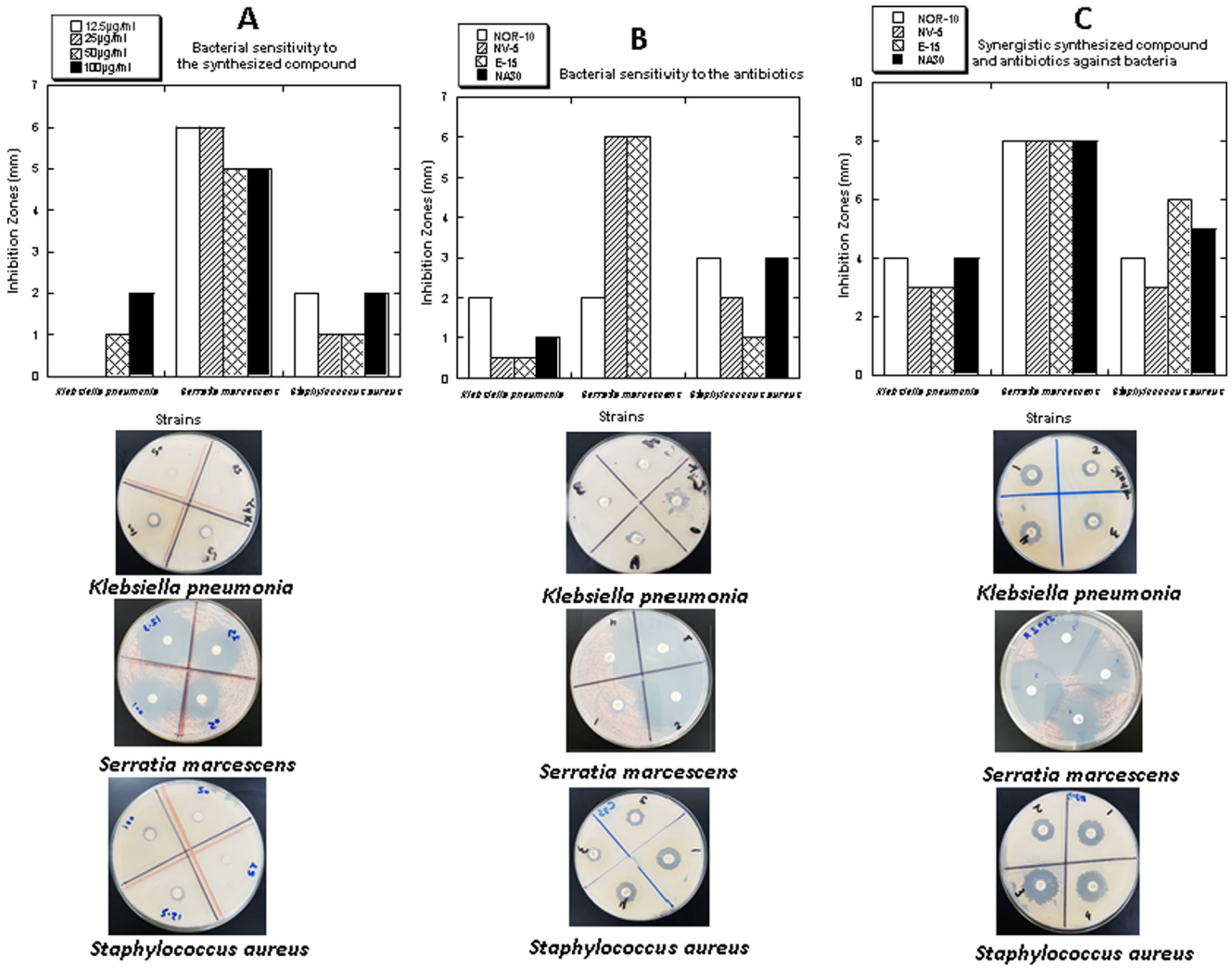


**Fig. 6.** A) Antimicrobial activity of the compound $(C_7H_{12}N_2)_2[CuCl_4]$; B) Antimicrobial activity of the antibiotics Norfloxacin (NOR-10), Novobiocin (NV-5), Erythromycin (E-15), and Nalidixic acid (NA30); C) Antimicrobial activity of the compound $(C_7H_{12}N_2)_2[CuCl_4]$ combined with the antibiotics.

## Declaration of Competing Interest

The authors declare that they have no known competing financial interests or personal relationships that could have appeared to influence the work reported in this paper.

## Acknowledgments


- The author would like to thank the Deanship of Scientific Research at Shaqra University for supporting this work.


## References


Al-Resayes, S.I., Azam, M., Alam, M., Kumar, R.S., Adil, S.F., 2017. Synthesis, crystal structure and Hirschfeld surface analyses of an alkyl amine based salt,$[C_5H_{16}N_2][ZnCl_4]$ and its enzyme inhibition activity. J. Saudi Chem. Soc. 21 (4), 481–486. https://doi.org/10.1016/j.jscs.2016.12.002.

Althobaiti, M.G., Hermi, S., Alotaibi, A.A., Alotaibi, K.M., Hassan, H.A., Mi, J.X., Nasr, C. B., Mrad, M.H., 2022. A New Cu (II) Metal Complex Template with 4–Tert–Butyl-Pyridinium organic cation: synthesis, structure, hirshfeld surface, characterizations and antibacterial activity. Crystals 12 (2), 254. https://doi.org/10.3390/cryst12020254.

Anjaneyulu, Y., Prabhakara Rao, R., 1986. Preparation, characterization and antimicrobial activity studies on some ternary complexes of Cu(II) with acetylacetone and various salicylic acids. Synth. React. Inorg. Met. Org. Chem 16 (2), 257–272. https://doi.org/10.1080/00945718608057530.

Azam, M., Wabaidur, S.M., Alam, M., Khan, Z., Alanazi, I.O., Al-Resayes, S.I., Moon, I. S., 2021. Synthesis, characterization, cytotoxicity, and molecular docking studies of ampyrone-based transition metal complexes. Transition Metal Chemistry 46, 65–71. https://doi.org/10.1007/s11243-020-00422-8.

Azam, M., Velmurugan, G., Trzesowska-Kruszynska, A., Al-Resayes, S.I., Kruszynski, R., Venuvanalingam, P., 2022. A bowl-shaped phenoxido-bridged binuclear zinc complex: experimental and theoretical studies. Inorganica Chimica Acta 534,. https://doi.org/10.1016/j.ica.2022.120807 120807.

Betteridge, P.W., Carruthers, J.R., Cooper, R.I., Prout, K., Watkin, D.J., 2003. J. Appl. Cryst. 36, 1487. https://doi.org/10.1107/S0021889803021800.

Buczkowska, M., Bodtke, A., Lindequist, U., Gdaniec, M., Bednarski, P.J., 2011. Cytotoxic and antimicrobial activities of Cu (II), Co (II), Pt (II) and Zn (II) complexes with N, O-Chelating heterocyclic carboxylates. Arch. Pharm 344 (9), 605–616. https://doi.org/10.1002/ardp.201100101.

Chalkha, M., el Hassani, A.A., Nakkabi, A., Tüzün, B., Bakhouch, M., Benjelloun, A.T., Sfaira, M., Saadi, M., El Ammari, L., El Yazidi, M., 2023. Crystal structure, Hirshfeld surface and DFT computations, along with molecular docking investigations of a new pyrazole as a tyrosine kinase inhibitor. J. Mol. Struct. 1273,. https://doi.org/10.1016/j.molstruc.2022.134255 134255.

Chandraleka, S., Ramya, K., Chandramohan, G., Dhanasekaran, D., Priyadharshini, A., Panneerselvam, A., 2014. Antimicrobial mechanism of copper (II) 1,10-phenanthroline and 2,2′-bipyridyl complex on bacterial and fungal pathogens. J. Saudi Chem. Soc 18 (6), 953–962. https://doi.org/10.1016/j.jscs.2011.11.020.

Duncan, C., White, A.R., 2012. Copper complexes as therapeutic agents. Metallomics 4 (2), 127–138. https://doi.org/10.1039/c2mt00174h.

Guan, A.Y., Liu, C.L., Sun, X.F., Xie, Y., Wang, M.A., 2016. Discovery of pyridine-based agrochemicals by using intermediate derivatization methods. Bioorg. Med. Chem. 24 (3), 342–353. https://doi.org/10.1016/j.bmc.2015.09.031.

Halvorson, K.E., Patterson, C., Willett, R.D., 1990. Structures of bis (4-aminopyridinium) tetrachlorocuprate (II) monohydrate,$[C_5H_7N_2]_2[CuCl_4]$. $H_2O$ and bis (2-amino-3-hydroxypyridinium) tetrachlorocuprate (II), $[C_5H_7N_2O]_2[CuCl_4]$: correlation of $CuCl_4^{2-}$ geometry with hydrogen bonding

and electronic structure. Acta. Crystallogr. B. Struct. Sci 46 (4), 508–519. https://doi.org/10.1107/S010876819000338X.
Hashem, H.E., Nath, A., Kumer, A., 2022. Synthesis, molecular docking, molecular dynamic, quantum calculation, and antibacterial activity of new Schiff base-metal complexes. J. Mol. Struct 1250,. https://doi.org/10.1016/j.molstruc.2021.131915 131915.
Himasekar, C., Mustafa, S., Babu, M.S., 2019. Synthesis, characterization of mixed Cu (II) PyridylTetrazoles and 1, 10-Phenanthroline complexes-DFT and biological activity. Open Chem. J 6 (1). https://doi.org/10.2174/1874842201906010001.
Kamat, V., Santosh, R., Poojary, B., Nayak, S.P., Kumar, B.K., Sankaranarayanan, M., Faheem, , Khanapure, S., Barretto, D.A., Vootla, S.K., 2020. Pyridine-and thiazole-based hydrazides with promising anti-inflammatory and antimicrobial activities along with their in silico studies. ACS omega 5 (39), 25228–25239. https://doi.org/10.1021/acsomega.0c03386.
Karaa, N., Hamdi, B., Salah, A.B., Zouari, R., 2012. Synthesis, infra-red, MAS-NMR characterization, structural study and electrical properties of the new compound $[C_5H_6ClN_2]_2Cd_3Cl_8$. J. Mol. Struct 1013, 168–176. https://doi.org/10.1016/j.molstruc.2011.12.053.
Khan, M.W., Mishra, R.P., Patel, B., Mishra, P., Vishwakarma, D., 2021. Importance of some transition metals and their biological role: a review. Int. Res. J. Pure Appl. Chem. https://doi.org/10.9734/IRJPAC/2021/v22i530406.
Krajčiová, D., Melník, M., Havránek, E., Forgácsová, A., Mikuš, P., 2014. Copper compounds in nuclear medicine and oncology. J. Coord. Chem 67 (9), 1493–1519. https://doi.org/10.1080/00958972.2014.915966.
Krasnovskaya, O., Naumov, A., Guk, D., Gorelkin, P., Erofeev, A., Beloglazkina, E., Majouga, A., 2020. Copper coordination compounds as biologically active agents. Int. J. Mol. Sci. 21 (11), 3965. https://doi.org/10.3390/ijms21113965.
Kumar, R., Kumar, A., Singh, R., Kashyap, R., Kumar, R., Kumar, D., Kumar, M., 2020. Selective room temperature ammonia gas detection using 2-amino pyridine functionalized graphene oxide. Mater. Sci. Semicond. Process 110,. https://doi.org/10.1016/j.mssp.2020.104920 104920.
Majerz, I., Malarski, Z., Sawka-Dobrowolska, W., 1995. Structure and IR Spectroscopic Properties of the Anhydrous 4-N, N-dimethylaminopyridinium Pentachlorophenolate. J. Chem. Crystallogr 25, 189–193. https://doi.org/10.1007/BF01666105.
Mali, S.N., Chaudhari, H.K., 2018. Computational studies on imidazo [1, 2-a] pyridine-3-carboxamide analogues as antimycobacterial agents: common pharmacophore generation, atom-based 3D-QSAR, molecular dynamics simulation, QikProp, molecular docking and prime MMGBSA approaches. Open Pharm. Sci. J 5 (1). https://doi.org/10.2174/1874844901805010012.
Mohammad Abu-Taweel, G., Ibrahim, M.M., Khan, S., Al-Saidi, H.M., Alshamrani, M., Alhumaydhi, F.A., Alharthi, S.S., 2022. Medicinal importance and chemosensing applications of pyridine derivatives: a review. Crit. Rev. Anal. Chem 1–18. https://doi.org/10.1080/10408347.2022.2089839.
Munawar, K.S., Ali, S., Muhammad, S., Ashfaq, M., Abbas, S.M., Tahir, M.N., Siddeeg, S.M., Ahmed, G., 2023. Synthesis, crystal structure, Hirshfeld surface analysis, DNA binding, optical and nonlinear optical properties of Schiff bases derived from o-aminophenol. J. Mol. Struct. 1274,. https://doi.org/10.1016/j.molstruc.2022.134427 134427.
Nasr, M.B., Kaabi, K., Zeller, M., Fujita, W., da Silva, P.S.P., Nasr, C.B., 2016. Synthesis, crystal structure, magnetic properties and second harmonic generation of a new noncentrosymmetric coordination compound: Triaqua (4-amino-6-methoxypyrimidine) cuprate (II) sulfate. Chin. Chem. Lett 27 (6), 896–900. https://doi.org/10.1016/j.cclet.2016.02.024.
Oliveri, V., 2020. Biomedical applications of copper ionophores. Coord. Chem. Rev 422,. https://doi.org/10.1016/j.ccr.2020.213474 213474.
Prachayasittikul, S., Pingaew, R., Worachartcheewan, A., Sinthupoom, N., Prachayasittikul, V., Ruchirawat, S., Prachayasittikul, V., 2017. Roles of pyridine and pyrimidine derivatives as privileged scaffolds in anticancer agents. Mini-Rev. Med. Chem 17 (10), 869–901. https://doi.org/10.2174/1389557516666160923125801.
Psomas, G., 2020. Copper (II) and zinc (II) coordination compounds of non-steroidal anti-inflammatory drugs: Structural features and antioxidant activity. Coord. Chem. Rev 412,. https://doi.org/10.1016/j.ccr.2020.213259 213259.
Ragab, A., Ammar, Y.A., Ezzat, A., Mahmoud, A.M., Mohamed, M.B.I., Abdou, S., Farag, R.S., 2022. Synthesis, characterization, thermal properties, antimicrobial evaluation, ADMET study, and molecular docking simulation of new mono Cu (II) and Zn (II) complexes with 2-oxoindole derivatives. Comput. Biol. Med 145,. https://doi.org/10.1016/j.compbiomed.2022.105473 105473.
Robert, A., Liu, Y., Nguyen, M., Meunier, B., 2015. Regulation of copper and iron homeostasis by metal chelators: a possible chemotherapy for Alzheimer's disease. Acc. Chem. Res 48 (5), 1332–1339. https://doi.org/10.1021/acs.accounts.5b00119.
Sarangi, A.K., Mahapatra, B.B., Mohapatra, R.K., Sethy, S.K., Das, D., Pintilie, L., Kudrat-E-Zahan, M., Azam, M., Meher, H., 2020. Synthesis and characterization of some binuclear metal complexes with a pentadentate azodye ligand: an experimental and theoretical study. Applied Organometallic Chemistry 34 (8), e5693.
Schmidt, M.G., Tuuri, R.E., Dharsee, A., Attaway, H.H., Fairey, S.E., Borg, K.T., Salgado, C.D., Hirsch, B.E., 2017. Antimicrobial copper alloys decreased bacteria on stethoscope surfaces. Am. J. Infect. Control 45 (6), 642–647. https://doi.org/10.1016/j.ajic.2017.01.030.
Sheldrick, G.M., 2008. Acta Cryst. A64, 112–122. https://doi.org/10.1107/S0108767307043930.
Smolková, R., Zeleňák, V., Smolko, L., Sabolová, D., Kuchár, J., Gyepes, R., 2017. Novel Zn (II) complexes with non-steroidal anti-inflammatory ligand, flufenamic acid: characterization, topoisomerase I inhibition activity, DNA and HSA binding studies. J. Inorg. Biochem 177, 143–158. https://doi.org/10.1016/j.jinorgbio.2017.09.005.
Spackman, P.R., Turner, M.J., McKinnon, J.J., Wolff, S.K., Grimwood, D.J., Jayatilaka, D., Spackman, M.A., 2021. CrystalExplorer: a program for Hirshfeld surface analysis, visualization and quantitative analysis of molecular crystals. J. Appl. Crystallogr. 54, 1006–1011. https://doi.org/10.1107/S1600576721002910.
Sundaraganesan, N., Meganathan, C., Kurt, M., 2008. Molecular structure and vibrational spectra of 2-amino-5-methyl pyridine and 2-amino-6-methyl pyridine by density functional methods. J. Mol. Struct 891 (1–3), 284–291. https://doi.org/10.1016/j.molstruc.2008.03.051.
Sunitha, M., Venkateshappa, G., Ramesh, G., Kengaiah, J., Chandramohan, V., Shivananda, M.K., 2020. Synthesis, characterization, biological activities of novel tridentate ligand and its CU (II) 8 NI (II) complexes. J. Adv. Sci. Res 11 (Suppl 2), 154–161. https://doi.org/10.1016/j.arabjc.2010.05.001.
Szafran, M., Kowalczyk, I., Koput, J., Katrusiak, A., 2005. X-ray and DFT studies of the structure, vibrational and NMR spectra of 2-amino-pyridine betaine hydrochloride. J. Mol. Struct 744, 59–73. https://doi.org/10.1016/j.molstruc.2004.11.087.
Thanigaimani, K., Khalib, N.C., Temel, E., Arshad, S., Razak, I.A., 2015. New supramolecular cocrystal of 2-amino-5-chloropyridine with 3-methylbenzoic acids: Syntheses, structural characterization, Hirshfeld surfaces and quantum chemical investigations. J. Mol. Struct 1099, 246–256. https://doi.org/10.1016/j.molstruc.2015.06.015.
Vembu, N., Nallu, M., Garrison, J., Youngs, W.J., 2003. 4-Dimethylaminopyridinium Picrate: Supramolecular Aggregation through Extensive N—H...O and C—H...O Interactions. Acta Crystallogr. E 59, 913–916. https://doi.org/10.1107/S1600536803012212.
Wang, P., Yuan, Y., Xu, K., Zhong, H., Yang, Y., Jin, S., Yang, K., Qi, X., 2021. Biological applications of copper-containing materials. Bioact. Mater 6 (4), 916–927. https://doi.org/10.1016/j.bioactmat.2020.09.017.
Yang, L., Powell, D.R., Houser, R.P., 2007. Structural variation in copper (I) complexes with pyridylmethylamide ligands: structural analysis with a new four-coordinate geometry index, τ4. Dalton Trans 9, 955–964. https://doi.org/10.1039/B617136B.
Zakharychev, V.V., Kuzenkov, A.V., Martsynkevich, A.M., 2020. Good pyridine hunting: a biomimic compound, a modifier and a unique pharmacophore in agrochemicals. Chem. Heterocycl. Compd 56 (12), 1491–1516. https://doi.org/10.1007/s10593-020-02843-w.